Optimal fidelity of teleportation with continuous variables using three tunable parameters in a realistic environment

Li-Yun Hu,[1,2,*] Zeyang Liao,[1] Shengli Ma,[1] and M. Suhail Zubairy[1,†]
[1]*Institute for Quantum Science and Engineering (IQSE) and Department of Physics and Astronomy, Texas A&M University, College Station, Texas 77843, USA*
[2]*Center for Quantum Science and Technology, Jiangxi Normal University, Nanchang 330022, China*
(Received 2 October 2015; published 2 March 2016)

We introduce three tunable parameters to optimize the fidelity of quantum teleportation with continuous variables in a nonideal scheme. By using the characteristic-function formalism, we present the condition that the teleportation fidelity is independent of the amplitude of input coherent states for any entangled resource. Then we investigate the effects of tunable parameters on the fidelity with or without the presence of the environment and imperfect measurements by analytically deriving the expression of fidelity for three different input coherent-state distributions. It is shown that, for the linear distribution, the optimization with three tunable parameters is the best one with respect to single- and two-parameter optimization. Our results reveal the usefulness of tunable parameters for improving the fidelity of teleportation and the ability against decoherence.

DOI: 10.1103/PhysRevA.93.033807

I. INTRODUCTION

Quantum teleportation has an indispensable role in the manipulation of quantum states and the processing of quantum information [1–4]. Usually, the two-mode squeezed vacuum is often used as the entanglement resource with continuous variables (CVs). However, due to the limitation of experiments, it is hard to achieve a high degree of squeezing, which leads to a low teleportation fidelity.

In order to increase the entanglement and fidelity of teleportation, a number of methods have been proposed [5–14]. Among them, non-Gaussian operations, including the photon subtraction a or addition $a^\dagger$ or the superposition of both, can be used to realize this purpose for a given Vaidman–Brauntein–Kimble (VBK) scheme. For example, the superposition operator $ta^\dagger + ra$ is proposed for quantum-state engineering to transform a classical state into a nonclassical one [15], and it can also be applied on a two-mode squeezed vacuum (TMSV) for enhancing quantum entanglement as well as the fidelity of teleportation [16]. It is found that the fidelity of teleporting a coherent state can be further improved by optimizing the superposition operation compared with the other non-Gaussian states, such as photon-subtraction TMSV. As another example, a remarkable improvement of the teleportation fidelity with CVs can be obtained by optimizing a non-Gaussian resource in both the usual and nonideal VBK scheme [17–19]. In Ref. 18, the "shot fidelity" and single-gain factor are used to discuss the performance of teleportation. In fact, the protocols discussed above are employed to enhance the fidelity of teleportation by changing the quantum entangled resources.

Then an inverse question is that, given a certain class of entangled resources with some given properties, how can we modify the VBK scheme to improve the fidelity of teleportation? It is interesting to note that there is an alternative method to improve the fidelity of teleportation by using classical information. For instance, the fidelity of CV teleportation can be enhanced by tuning the gain parameters via Einstein-Podolsky-Rosen (EPR) resources without loss [7,20] and this has been experimentally realized by Furusawa *et al.* [21]. However, these two important theoretical works are concerned with the study of the ideal protocol implementation using Gaussian resources [7,20]. In addition, there are some other strategies by gain tuning and by gain optimization [22,23], using the Heisenberg picture and the Wigner function, but they cannot be directly applied to more general cases. In addition, in Refs. [22,24] the gain factor is used to maximize the teleportation fidelity for the case of Gaussian resources, but the gain-optimized fidelity of teleportation is strongly suppressed when dissipation is considered. Recently, a hybrid entanglement swapping protocol has been proposed experimentally to transfer discrete-variable (DV) entanglement by using continuous-variable (CV) Gaussian entangled resources and by tuning a gain factor of the teleporter [23,25,26], which shows that DV entanglement remains present after teleportation for any squeezing by optimal gain tuning. For more information about advances in quantum teleportation, we refer to a recent review paper [27] and references therein.

The fidelity of teleportation, as mentioned above, can be improved by using tunable entangled resources or classical parameters [17,18,20,23]. In Refs. [20,28], a three-parameter optimal strategy is introduced to improve the quality of teleportation, including unbalanced beam splitter (BS) and two nonunity gains. However, they only considered an ideal case. Actually, the interaction between the quantum system and the environment cannot be avoided and the Bell measurements are usually imperfect. Thus, it would be interesting to see whether it is still possible to enhance the fidelity by using these tunable parameters in a realistic case. In this paper, by using the characteristic-function (CF) formalism, we extend the analysis of the parameter-optimization strategy for realistic input states and nonideal entangled resources. We investigate nonideal quantum teleportation by deriving an analytical expression of the teleportation fidelity. This formalism is very convenient for discussing the teleportation for the nonideal case and any entangled resources.

This paper is arranged as follows: In Sec. II, we give a description of the characteristic-function formalism for

*hlyun2008@126.com
†zubairy@physics.tamu.edu

the case of the nonideal CV teleportation scheme. In this scheme, we find the condition that the fidelity is independent of the amplitude of input coherent states for any entangled resource. Then we present a qualitative description of fidelity and average fidelity. In Sec. III, we derive an analytical expression of the fidelity of teleportation when the TMSV and coherent states are used as entangled channel and teleported states, respectively. In Sec. IV we study the performance of amplitude-independent optimal fidelity by using the condition found in Sec. II. It is found that the optimal condition is just that the two gain factors and θ are equal to unity and $\pi/4$, respectively. Section V is devoted to discussing the optimal fidelity over these three tunable parameters and three different probability distributions for the input coherent states by deriving the analytical expression of the optimal fidelity. Our conclusions are drawn in the last section.

II. MODE AND QUANTITATIVE ANALYSIS

Here, we consider a more realistic case of the teleportation scheme shown in Fig. 1(a). In this scheme, there are three tunable parameters, unbalanced BS and two nonunity gains (g_q and g_p). The input state (mode 1) and the entangled resources (shared by modes 2 and 3) are not limited to being pure states. Considering that mode 2 can be prepared close to the sender Alice while mode 3 usually has to propagate over much longer distances, we can assume that mode 2 is not affected by losses but that mode 3 is. In addition, two symmetrical lossy bosonic channels have been considered before making Bell measurements, which are simulated through an extra vacuum mode and a beam splitter with transmission coefficient T. The input states of modes 4 and 5 are pure vacuum states.

Next, we describe the scheme in the CF formalism where it is very convenient to discuss teleportation for the nonideal case and for non-Gaussian entangled resources [18,29].

A. Input-output relation of beam splitter in characteristic-function formalism

To obtain the relationship between input and output, we first calculate the output of a beam splitter with a vacuum and an arbitrary density operator as inputs shown in Fig. 1(b). For simplicity, we denote the vacuum and the input state as $|0\rangle_5$ and ρ_1, respectively. The output state (denoted as ρ_1') is given by

$$\rho_1' = \mathrm{Tr}_5[B_{15}(T)\rho_1 \otimes |0\rangle_{5,5}\langle 0|B_{15}^\dagger(T)], \tag{1}$$

where Tr_5 is the partial trace over the ancilla mode 5 and $B_{kl}(T) = \exp[\varphi(a_k a_l^\dagger - a_k^\dagger a_l)]$ is the beam-splitter operator describing the interaction between modes 1 and 5 with $\cos\varphi = \sqrt{T}$ and $a_{k,l}$ $(k = 1, l = 5)$ being the photon annihilation operator of the $k(l)$ modes. By using the Weyl expansion of the density operator, we can express the density operator ρ_1 and the vacuum projector $|0\rangle_{55}\langle 0|$ in the following forms:

$$\rho_1 = \int \frac{d^2\alpha}{\pi}\chi_1(\alpha)D_1(-\alpha),$$
$$|0\rangle_{55}\langle 0| = \int \frac{d^2\beta}{\pi}e^{-\frac{1}{2}|\beta|^2}D_5(-\beta), \tag{2}$$

where $D_1(\alpha) = \exp\{\alpha a_1^\dagger - \alpha^* a_1\}$ is the displacement operator, and $\chi_1(\alpha)$ is the CF of ρ_1. On the other hand, by using the transformation relation

$$B_{15}D_1(-\alpha)D_5(-\beta)B_{15}^\dagger = D_1(\bar{\alpha})D_5(\bar{\beta}), \tag{3}$$

where $R = 1 - T$, $\bar{\alpha} = \beta\sqrt{R} - \alpha\sqrt{T}$, and $\bar{\beta} = -\beta\sqrt{T} - \alpha\sqrt{R}$, we can derive

$$\begin{aligned}\mathrm{Tr}_5[B_{15}D_1(-\alpha)D_5(-\beta)B_{15}^\dagger] &= D_1(\bar{\alpha})\mathrm{Tr}_5[D_5(\bar{\beta})] \\ &= D_1(\bar{\alpha})\pi\delta^{(2)}(\bar{\beta}).\end{aligned} \tag{4}$$

Here we have used the relation $\mathrm{Tr}_5 D_5(\bar{\beta}) = \pi\delta^{(2)}(\bar{\beta})$. Substituting Eqs. (2) and (4) into Eq. (1) then yields

$$\begin{aligned}\rho_1' &= \int \frac{d^2\alpha d^2\beta}{\pi^2}e^{-\frac{1}{2}|\beta|^2}\chi_1(\alpha)\mathrm{Tr}_5[D_1(\bar{\alpha})D_5(\bar{\beta})] \\ &= \int \frac{d^2\alpha d^2\beta}{\pi^2}e^{-\frac{1}{2}|\beta|^2}\chi_1(\alpha)D_1(\bar{\alpha})\pi\delta^{(2)}(\bar{\beta}) \\ &= \int \frac{d^2\alpha}{\pi}e^{-\frac{1}{2}R|\alpha|^2}\chi_1(\sqrt{T}\alpha)D_1(-\alpha),\end{aligned} \tag{5}$$

where $e^{-\frac{1}{2}|\beta|^2}$ is the CF of the vacuum state, and in the second step in Eq. (5) the CF $\chi_1(\alpha)$ is transformed to $\chi_1(\sqrt{T}\alpha)$ with a Gaussian term $e^{-\frac{1}{2}R|\alpha|^2}$ due to photon loss. It is then convenient to obtain the input-output relation of the teleportation scheme shown in Fig. 1(a) as detailed below.

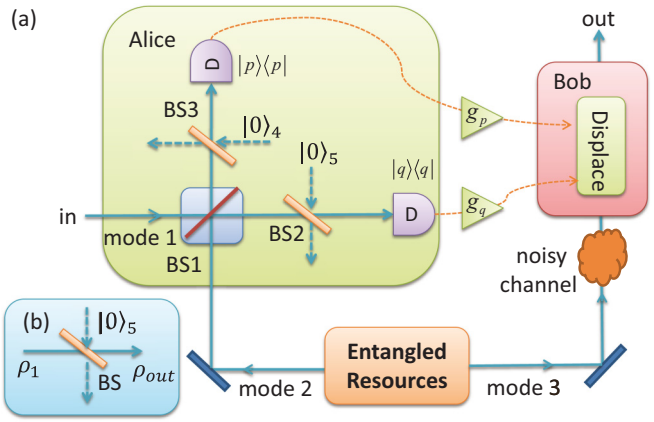

FIG. 1. Realistic schematic diagram for CV teleportation. "BS" indicates beam splitter.

B. Input-output relation of teleportation scheme in characteristic-function formalism including photon loss or imperfect Bell measurements

Next, we consider the effect of photon loss on the relation between input and output of the teleportation scheme in CF formalism. Here we use BS2 and BS3 with vacuum inputs to simulate the photon loss or imperfect Bell measurements [see Fig. 1(b)] and denote the teleported state, entangled resource, and auxiliary vacuum as ρ_1, ρ_{23}, and $|00\rangle_{45}$, respectively. To realize the teleportation, Alice should make Bell measurements on modes 1 and 2. Before she makes the Bell measurements, the unitary-state evolution can be formulated as

$$\rho_{1-5} = U\rho_1 \otimes \rho_{23} \otimes |00\rangle_{45}\langle 00|U^\dagger, \tag{6}$$

where the unitary evolution operator is defined as $U. = .B_{24}B_{15}B_{12}$ and B_{kl} are the BS operators defined as before. In a similar way as for deriving Eq. (5), and using the Weyl expansion for the entangled resource, the reduced output state denoted as $\rho_{1-3} \equiv \mathrm{Tr}_{45}\rho_{1-5}$ is given by

$$\begin{aligned}\rho_{1-3} &= \mathrm{Tr}_{45}[U\rho_1 \otimes \rho_{23} \otimes |00\rangle_{45}\langle 00|U^\dagger] \\ &= \int \frac{d^2\alpha d^2\beta d^2\gamma}{\pi^3}\chi_1(\alpha)\chi_{23}(\beta,\gamma) \\ &\quad \times \mathrm{Tr}_{45}[U D_1(-\alpha)D_2(-\beta)D_3(-\gamma)|00\rangle_{45}\langle 00|U^\dagger] \\ &= \int \frac{d^2\alpha d^2\beta d^2\gamma}{\pi^3}\chi_1(\alpha)\chi_{23}(\beta,\gamma)\mathrm{Tr}_{45}[B_{24} \\ &\quad \times B_{15}D_1(-\alpha_1)D_2(-\beta_1)D_3(-\gamma)|00\rangle_{45}\langle 00|B_{24}^\dagger B_{15}^\dagger], \end{aligned} \tag{7}$$

where $B_{12}D_1(-\alpha)D_2(-\beta)B_{12}^\dagger = D_1(-\alpha_1)D_2(-\beta_1)$ with $\alpha_1 = \alpha\cos\theta - \beta\sin\theta$, $\beta_1 = \beta\cos\theta + \alpha\sin\theta$, and $\cos^2\theta$ being the transmission coefficient of beam splitter B_{12}. By using Eqs. (1) and (4), we can obtain

$$\begin{aligned}\rho_{1-3} &= \int \frac{d^2\alpha d^2\beta d^2\gamma}{\pi^3}\chi_1(\sqrt{T}\alpha)\chi_{23}(\sqrt{T}\beta,\gamma) \\ &\quad \times e^{-\frac{R}{2}(|\alpha_1|^2+|\beta_1|^2)}D_1(-\alpha_1)D_2(-\beta_1)D_3(-\gamma). \end{aligned} \tag{8}$$

Equation (8) is the representation in CF of the deduced density operator before Bell measurements but after BS2 and BS3.

Then, as the first step of teleportation, Alice makes a joint measurement for modes 1 and 2 at the output ports, i.e., measures two observables corresponding to coordinate and momentum of modes 1 and 2. After the measurements, the outcomes ρ_M (M means measurement) in mode 3 are

$$\rho_M \equiv \frac{1}{P(q,p)}\mathrm{Tr}_{12}[|q\rangle_{11}\langle q| \otimes |p\rangle_{22}\langle p|\rho_{1-3}], \tag{9}$$

where $P(q,p)$ is the probability distribution function of the Bell measurement outcomes, $P(q,p) = \mathrm{Tr}_3\{\mathrm{Tr}_{12}[|q\rangle_{11}\langle q| \otimes |p\rangle_{22}\langle p|\rho_{1-3}]\}$, and $|q\rangle_1$ and $|p\rangle_2$ are the eigenstates of coordinate and momentum operators Q_1 and P_2 corresponding to modes 1 and 3, respectively.

According to the definition of the CF and using the relations

$$\begin{aligned}\mathrm{Tr}_1[|q\rangle_{1,1}\langle q|D_1(\alpha)] &= e^{i\sqrt{2}q\,\mathrm{Im}\,\alpha}\delta(\sqrt{2}\,\mathrm{Re}\,\alpha), \\ \mathrm{Tr}_2[|p\rangle_{2,2}\langle p|D_2(\beta)] &= e^{-i\sqrt{2}p\,\mathrm{Re}\,\beta}\delta(\sqrt{2}\,\mathrm{Im}\,\beta), \end{aligned} \tag{10}$$

and

$$\mathrm{Tr}_3[D_3(-\gamma)D_3(\eta)] = \pi\delta^{(2)}(\eta-\gamma), \tag{11}$$

the CF of ρ_M defined as $\chi_M(q,p;\eta) = \mathrm{Tr}_3[\rho_M D_3(\eta)]$ reads

$$\begin{aligned}\chi_M(q,p;\eta) &= \frac{P^{-1}(q,p)}{\sin 2\theta}\int\frac{d^2\alpha}{\pi^2}\exp\{\alpha^*\xi - \alpha\xi^*\} \\ &\quad \times \chi_1(\sqrt{T}\alpha)\chi_{23}[\sqrt{T}(\alpha\cot 2\theta + \alpha^*\csc 2\theta),\eta] \\ &\quad \times \exp\left\{-\frac{R}{2}[(\mathrm{Re}\,\alpha)^2\csc^2\theta \right. \\ &\quad \left. + (\mathrm{Im}\,\alpha)^2\sec^2\theta]\right\}, \end{aligned} \tag{12}$$

where we have defined $\xi = (q/\cos\theta + ip/\sin\theta)/\sqrt{2}$. When $T = 1$, Eq. (12) reduces to Eq. (2.9) in Ref. [29].

After Alice communicates the measured results (q,p) to Bob, Bob needs to make a unitary transformation on mode 3 to obtain the output state of the teleportation. Here, we consider the unitary transformation to be the displacement operator $D_3(Z)$ with nonunity and asymmetrical gains, where $Z \equiv g_q q + ig_p p$ with g_q and g_p being two tunable gain parameters. Thus, after the displacement operation, the output state can be expressed as $\rho_D \equiv \int d^2\eta\chi_M(q,p;\eta)D_3(Z)D_3(-\eta)D_3(-Z)/\pi$. Usually, we are not interested in every measurement result but the average effect. Thus, we perform an ensemble averaging over all measurement results, and the average CF of the output state $\bar{\chi}_{\mathrm{out}}$ is given by

$$\begin{aligned}\bar{\chi}_{\mathrm{out}}(\beta) &= \mathrm{Tr}_3\left[D_3(\beta)\int dqdpP(q,p)\rho_D\right] \\ &= \chi_1(f_1\beta - f_2\beta^*)\chi_{23}(\beta^* f_3 - \beta f_4,\beta) \\ &\quad \times \exp\left\{-R\left[g_p^2(\mathrm{Re}\,\beta)^2 + g_q^2(\mathrm{Im}\,\beta)^2\right]\right\}, \end{aligned} \tag{13}$$

where

$$\begin{aligned} f_1 &= \sqrt{\frac{T}{2}}(g_q\cos\theta + g_p\sin\theta), \\ f_2 &= \sqrt{\frac{T}{2}}(g_q\cos\theta - g_p\sin\theta), \\ f_3 &= \sqrt{\frac{T}{2}}(g_q\sin\theta + g_p\cos\theta), \\ f_4 &= \sqrt{\frac{T}{2}}(g_q\sin\theta - g_p\cos\theta), \end{aligned} \tag{14}$$

and T (R) denotes the transmissivity (reflectivity) of BS2 and BS3 with $T + R = 1$, which can simulate the photon losses or the imperfect Bell measurements.

C. Relation between input and output in characteristic-function formalism including noise in mode 3

In this section, we consider the effect of decoherence of mode 3 in the CF formalism. Here we consider the case where mode 3 propagates in a noisy channel such as photon loss and thermal noise. We assume that the decoherence occurs after Alice's measurement but before it reaches Bob's location [see Fig. 1(a)]. In the interaction picture and the Born–Markov approximation, the time evolution of the density matrix describing the thermal environment is governed by the master equation (ME) [30]

$$\begin{aligned}\frac{d}{dt}\rho(t) &= \kappa\bar{n}(2a^\dagger\rho a - aa^\dagger\rho - \rho aa^\dagger) \\ &\quad + \kappa(\bar{n}+1)(2a\rho a^\dagger - a^\dagger a\rho - \rho a^\dagger a), \end{aligned} \tag{15}$$

where κ is the dissipative coefficient and $\bar{n}$ is the average thermal photon number of the environment. When $\bar{n} = 0$, Eq. (15) reduces to the one describing the photon-loss channel. By solving the ME in the CF form, one can find that the evolution of the CF described by Eq. (15) is given by

$$\chi(\gamma;t) = \chi(\gamma e^{-\kappa t};0)\exp\{-\Gamma|\gamma|^2\}, \tag{16}$$

where $\Gamma = (2\bar{n}+1)(1-e^{-2\kappa t})/2$, and $\chi(\gamma;0)$ is the CF of the initial state $\rho(0)$. In a similar way as for deriving Eq. (13), the CF $\bar{\chi}_f$ of the final output state including the decoherence on mode 3 can be calculated to be

$$\bar{\chi}_f(\beta;t) = e^{-\Gamma|\beta|^2}\chi_1(f_1\beta - f_2\beta^*)\chi_{23}(\beta^* f_3 - \beta f_4, \beta e^{-\kappa t}) \times \exp\left\{-R\left[g_p^2(\mathrm{Re}\,\beta)^2 + g_q^2(\mathrm{Im}\,\beta)^2\right]\right\}. \quad (17)$$

From Eq. (17), one can see the different roles played by the noise channel (Γ,κ), gain factors (g_p,g_q), as well as the unbalanced BS (θ) and the reflectivity R. The decoherence effect from the noisy channel affects only mode 3 by means of the exponentially decreasing weight $e^{-\kappa t}$ in the arguments of χ_{23}. Equation (17) is the general description of the input-output relations of the nonideal teleportation scheme in CF formalism, which reduces to the factorized form of the output CF in Eq. (9) herein and in Eq. (4) of Ref. [18], as expected, when $\kappa t = 0$ and $g_q = g_p = g$, $\theta = \pi/4$, respectively.

D. Fidelity and average fidelity

To measure the performance of the teleportation scheme, we resort to the fidelity of teleportation, defined by $\mathcal{F} = \mathrm{Tr}(\rho_{\mathrm{in}}\rho_{\mathrm{out}})$, *which is valid only for the pure input or output states*. In the CF formalism, the fidelity reads

$$\mathcal{F} = \int \frac{d^2\lambda}{\pi}\chi_{\mathrm{in}}(\lambda)\chi_{\mathrm{out}}(-\lambda), \quad (18)$$

where χ_{in} and χ_{out} are the CFs corresponding to density operators ρ_{in} and ρ_{out}, respectively. Equation (18) is the fundamental quantity that measures the performance of a CV teleportation, which is often used in the following calculations. Based on Eqs. (17) and (18), we can examine the performance of teleportation for pure input states and any entangled resources, including non-Gaussian ones.

In particular, when we specify the input teleported states at Alice's location to be coherent states $\rho_1 = |\epsilon\rangle\langle\epsilon|$ with complex amplitude ϵ, the CF reads $\chi_1(\lambda) = e^{-\frac{1}{2}|\lambda|^2+\lambda\epsilon^*-\epsilon\lambda^*}$. By substituting $\chi_1(\lambda)$ into Eqs. (17) and (18) we get

$$\mathcal{F} = \int \frac{d^2\lambda}{\pi}\exp\left\{-\frac{1}{2}\left(1+f_1^2+f_2^2+2\Gamma\right)|\lambda|^2\right\} \times \exp\left\{\frac{1}{2}f_1f_2(\lambda^2+\lambda^{*2}) + \lambda\Delta - \lambda^*\Delta^*\right\} \times \chi_{23}(\lambda f_4 - \lambda^* f_3, -\lambda e^{-\kappa t}) \times \exp\left[-R\left(g_p^2\,\mathrm{Re}^2\,\lambda + g_q^2\,\mathrm{Im}^2\,\lambda\right)\right], \quad (19)$$

where $\Delta = (1-f_1)\epsilon^* - \epsilon f_2$. The amplitude of the coherent state only appears in the parameter Δ. If we choose $\Delta = 0$ then the fidelity will be independent of ϵ for any entangled resources. The conditions of $\Delta = 0$ are given by

$$g_q = \frac{1}{\sqrt{2T}\cos\theta}, \quad g_p = \frac{1}{\sqrt{2T}\sin\theta}. \quad (20)$$

This is the only choice making the fidelity independent of ϵ, which allows us to have no information about the input coherent states. The conditions shown in Eq. (20) depend on T and θ but are independent of the decoherence involved in mode 3. This is true for any entangled resources. In particular, when $\theta = \pi/4$, Eq. (20) reduces to the case in Ref. [18]; while for $T = 1$ and $\theta = \pi/4$, this result is just the case discussed in Ref. [31].

In general, the fidelity in Eq. (19) depends on the teleported input states which are usually unknown by the sender and the receiver. Here, we introduce the average fidelity to describe the performance of a teleportation scheme with unknown inputs. Assuming that partial knowledge of the input states is known, e.g., the probability distribution of the input states is given by $P(\mu)$ with $\int P(\mu)d\mu = 1$ where the integral is taken over all possible values of μ, the average fidelity is then given by

$$\bar{F} = \int \mathcal{F}(\mu)P(\mu)d\mu. \quad (21)$$

In the following sections, we take three probability distributions into account for input coherent states, such as line-, circle- and two-dimensional Gaussian distributions [20].

III. TWO-MODE SQUEEZED VACUUM AS ENTANGLED RESOURCES

In this section, we use the usual TMSV as entangled resources to analyze the performance of these three tunable parameters for improving the fidelity of teleportation. The TMSV entangled resource, most commonly used in continuous-variable teleportation, can be generated by the parametric down-conversion (PDC) process and theoretically can be defined as

$$|\Phi\rangle_{sv} = S(r)|00\rangle = \mathrm{sech}r\exp(a^\dagger b^\dagger \tanh r)|00\rangle, \quad (22)$$

where $S(r) = \exp\{r(a^\dagger b^\dagger - ab)\}$ is the two-mode squeezing operator with r being the squeezing parameter, and $a^\dagger(a)$ and $b^\dagger(b)$ are photon creation (annihilation) operators. According to the definition of the CF, the CF of the TMSV is given by

$$\chi_{sv}(\alpha,\beta) = \exp\left\{-\tfrac{1}{2}(|\alpha|^2+|\beta|^2)\cosh 2r\right\} \times \exp\left\{\tfrac{1}{2}(\alpha\beta+\alpha^*\beta^*)\sinh 2r\right\}. \quad (23)$$

In particular, for the largest entangled resource with $r\to\infty$, we have $\lim_{r\to\infty}\chi_{sv}(\beta^*,\beta) = 1$. For ideal Bell measurements with $T = 1$ and $R = 0$, as well as balanced BSs $(\theta = \pi/4)$ and $g_1 = g_2 = 1$, we have $f_1 = f_3 = 1$ and $f_2 = f_4 = 0$. Substituting these into Eq. (13) yields $\lim_{r\to\infty}\bar{\chi}_{\mathrm{out}}(\beta) = \chi_1(\beta)$, i.e., a perfect teleportation fidelity is achieved, as expected.

When Alice uses the TMSV as entangled resource to teleport the coherent states, the fidelity in Eq. (19) can be calculated as

$$\mathcal{F} = \frac{1}{\sqrt{G}}\exp\left\{\frac{-K_1|\Delta|^2 + K_2(\Delta^2+\Delta^{*2})}{G}\right\}, \quad (24)$$

where we have defined $G = K_1^2 - 4K_2^2$ and

$$K_1 = \frac{1}{2}\left(1+f_1^2+f_2^2+2\Gamma\right) + \frac{R}{2}\left(g_p^2+g_q^2\right) + \frac{1}{2}\left(f_3^2+f_4^2+e^{-2\kappa t}\right)\cosh 2r - f_3e^{-\kappa t}\sinh 2r,$$

$$K_2 = \frac{1}{2}\left\{f_1f_2 - R\left(g_p^2-g_q^2\right)/2 + f_3f_4\cosh 2r - f_4e^{-\kappa t}\sinh 2r\right\}, \quad (25)$$

and have used the following integration formula:

$$\int \frac{d^2z}{\pi} \exp(\zeta|z|^2 + \xi z + \eta z^* + f z^2 + g z^{*2}) = \frac{1}{\sqrt{\zeta^2 - 4fg}} \exp\left\{\frac{-\zeta\xi\eta + \xi^2 g + \eta^2 f}{\zeta^2 - 4fg}\right\}. \quad (26)$$

From Eq. (24) one can see that the fidelity $\mathcal{F}$ depends on the amplitude of the teleported coherent states. In the next sections, we consider two kinds of cases: one is independent of the amplitude by the choice in Eq. (20) and the other is not, but partial information about the input-state distribution is known.

IV. ϵ-INDEPENDENT OPTIMAL FIDELITY

In this section, we examine the fidelity for teleporting coherent states with two gain factors fixed to be $g_q = 1/(\sqrt{2T}\cos\theta)$, $g_p = 1/(\sqrt{2T}\sin\theta)$. This choice allows us to have no information about the amplitude of coherent states. Noticing that $f_1 = 1$, $f_2 = 0$, $f_3 = \csc 2\theta$, and $f_4 = -\cot 2\theta$, then from Eq. (24) we get

$$\mathcal{F}_\epsilon = \{H[1/(\sqrt{2T}c_1), c_2]H[1/(\sqrt{2T}c_2), c_1]\}^{-1/2}, \quad (27)$$

where $c_1 = \cos\theta$, $c_2 = \sin\theta$, and we define the function $H(x,y)$ as

$$H(x,y) = \tfrac{1}{2} + \Gamma + x^2(1 + 2Ty^2\sinh^2 r) + \tfrac{1}{2}e^{-2\kappa t}\cosh 2r - xye^{-\kappa t}\sqrt{2T}\sinh 2r. \quad (28)$$

It is clear that the fidelity $\mathcal{F}_\epsilon$ depends on multiparameters such as r, κt, $\bar{n}$, T, and θ. At fixed r, κt, $\bar{n}$, and T, the optimal fidelity of teleportation is defined as

$$\mathcal{F}_{\rm opt} = \max_\theta \mathcal{F}(r,\theta). \quad (29)$$

To maximize the fidelity in Eq. (27) over θ, we can take $\partial\mathcal{F}_\epsilon/\partial\theta = 0$, which leads to the condition

$$\cos 2\theta = 0, \quad (30)$$

or

$$\csc 2\theta = \frac{1}{2}\left\{\frac{e^{-\kappa t}\sinh 2r}{1/T + 2\sinh^2 r} + \frac{e^{-\kappa t}\sinh 2r}{1/T + 1 + 2\Gamma + e^{-2\kappa t}\cosh 2r}\right\}. \quad (31)$$

It is not difficult to see that the first term (F_1) in the curly bracket of Eq. (31) is less than unity, and the second term (F_2) satisfies (by taking $T = 1$ and $\bar{n} = 0$)

$$\frac{e^{-\kappa t}\sinh 2r}{1/T + 1 + 2\Gamma + e^{-2\kappa t}\cosh 2r} \leqslant \frac{e^{-\kappa t}\sinh 2r}{3 + 2e^{-2\kappa t}\sinh^2 r}. \quad (32)$$

By numerical calculation, we find that, when the squeezing parameter r is less than a threshold value of about 2.1, the sum of $(F_1 + F_2)/2$ is always less than unity, which will lead to an impossible case, i.e., $\csc 2\theta < 1$. Thus, within the region of the threshold value, the optimal point is at $\theta = \pi/4$ and $g_q = g_p = 1/\sqrt{T}$, which is independent of $\bar{n}$ and $e^{-\kappa t}$. The threshold value of r will increase with increasing $\bar{n}$ and $1/T$. Actually, the presence of the threshold value results from the decoherence on mode 3, since F_2 is always less than unity for any squeezing r when $\kappa t = 0$.

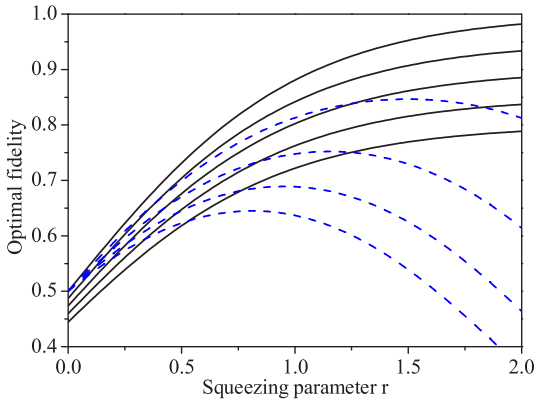

FIG. 2. The optimal fidelity for teleporting coherent states as a function of the squeezing parameter r with some different values of T and κt when $\bar{n} = 0$. Here, solid lines are the transmissivity $T = 1$, 0.95, 0.9, 0.85, 0.8 and $\kappa t = 0$. Blue-dash lines are $\kappa t = 0.1$, 0.2, 0.3, 0.4 and $T = 1$. The corresponding lines are arranged from top to bottom with the increasing $1/T$ and κt, respectively.

Substituting the above optimal condition into Eq. (27), we get the optimal fidelity

$$\mathcal{F}_{\rm opt} = \left[\frac{1}{T} + \Gamma + e^{-\kappa t}(\cosh\kappa t\cosh 2r - \sinh 2r)\right]^{-1}. \quad (33)$$

It is clear that $\mathcal{F}_{\rm opt}$ decreases with the increasing $\bar{n}$ and $1/T$, as expected. In particular, when $\kappa t = 0$ and $T = 1$, Eq. (33) reduces to $\mathcal{F}_{\rm opt} = (1 + \tanh r)/2$, which is the best fidelity when we use the coherent states as inputs and the TMSV as entangled resources in the VBK scheme. In addition, when $\kappa t \to \infty$, $\mathcal{F}_{\rm opt} \to (\frac{1}{T} + \bar{n} + \cosh^2 r)^{-1}$, which decreases with the increasing $\bar{n}$, r and the decreasing T.

In order to examine the effects of different parameters on the optimal fidelity, we plot the optimal fidelities as a function of squeezing parameter r for different κt and T in Fig. 2. From Fig. 2, we can see that, for $\kappa t = 0$ (without decoherence on mode 3), the optimal fidelities increase monotonically with the increasing squeezing parameter r and the transmissivity T. However, when we consider the effects of decoherence on mode 3, the optimal fidelities first increase and then decrease with the increasing r. The maximal value and the corresponding value of $r_{\rm max}$ reduces as κt increases. In fact, we can take $\partial\mathcal{F}_{\rm opt}/\partial r = 0$ to get the following simple expression for $r_{\rm max}$ ($\cosh\kappa t = \coth 2r_{\rm max}$):

$$e^{2r_{\rm max}} = \coth\frac{\kappa t}{2}. \quad (34)$$

It is interesting to note that $r_{\rm max}$ is independent of T and $\bar{n}$.

V. AVERAGE OPTIMAL FIDELITY AND EFFECT OF TUNABLE PARAMETERS

In the previous section, we considered the ϵ-independent optimal fidelity. However, when $g_q \neq 1/(\sqrt{2T}\cos\theta)$ and $g_p \neq 1/(\sqrt{2T}\sin\theta)$, the scenario is changed dramatically. In this case, the fidelity in Eq. (24) depends on the amplitude ϵ of the coherent state. In this section, we examine the average

optimal fidelity for three different probability distributions of the teleported input states where partial information of the input state is known by Alice and Bob. For example, they may be completely sure of the phase of the input states but the amplitude is unknown [20].

A. Optimal fidelity for teleporting coherent states on a line

First, let us consider the teleportation of coherent states on a line, i.e., the phase is fixed but the amplitude can vary. Without loss of generality, we assume here that the phase of the teleported coherent states is zero because we can always achieve this by rotating frame. The corresponding probability distribution can be given by (letting $\epsilon = x + iy$)

$$P(x,y) = \frac{1}{2L}\delta(y) \times \begin{cases} 1, & |x| \leqslant L \\ 0, & \text{otherwise.} \end{cases} \tag{35}$$

Substituting Eqs. (24) and (35) into Eq. (21) yields the average fidelity

$$\begin{aligned} \bar{\mathcal{F}}_{\text{line}} &= \frac{1}{2L\sqrt{G}} \int_{-L}^{L} dx e^{-\frac{M}{G}x^2} \\ &= \frac{\sqrt{\pi}}{2L\sqrt{M}} \text{Erf}\left\{ \frac{|1-\sqrt{2T}g_q \cos\theta|}{[H(g_q,\sin\theta)]^{1/2}L^{-1}} \right\}, \end{aligned} \tag{36}$$

where $\text{Erf}\{a\} = 1/\sqrt{\pi}\int_{-a}^{a} e^{-x^2}dx$ is the error function and $M\cdot = \cdot(1-\sqrt{2T}g_q\cos\theta)^2 H(g_p,\cos\theta)$.

Noticing the separability of g_q and g_p in $\bar{\mathcal{F}}_{\text{line}}$, the optimal value of g_p can be obtained by $\partial\bar{\mathcal{F}}_{\text{line}}/\partial g_p = 0$ equivalent to $\partial H(g_p,\cos\theta)/\partial g_p = 0$, which leads to

$$g_p^{\text{opt}} = \frac{e^{-\kappa t}\sqrt{2T}\cos\theta^{\text{opt}}\sinh 2r}{2(1+2T\cos^2\theta^{\text{opt}}\sinh^2 r)}. \tag{37}$$

It is interesting to note that the optimal value of g_p^{opt} is related to $e^{-\kappa t}$ and T but independent of the average thermal-photon number. In particular, for the ideal case of $\kappa t = 0$ and $T = 1$, Eq. (37) just reduces to Eq. (27) in Ref. [28], except for a factor $\sqrt{2}$ which is from the different definition of gain factors.

Next, we maximize the fidelity by numerical calculation. At fixed r, κt, $\bar{n}$, and T, the optimal fidelity of teleportation can be defined as

$$\bar{\mathcal{F}}_{\text{line}}^{\text{opt}} = \max_{g_q,g_p,\theta} \bar{\mathcal{F}}_{\text{line}}(r,g_q,g_p,\theta). \tag{38}$$

In Fig. 3 we plot the optimal fidelity as a function of squeezing parameter r for some different values of parameters κt, $\bar{n}$, and T. In Fig. 3(a), we consider the optimal fidelities with some different values of L and $T = 1$, $\bar{n} = 0$ as well as $\kappa t = 0.2$ (for comparison, the case of $\kappa t = 0$ is also plotted as dashed lines). From Fig. 3(a), we can see that the optimal fidelities grow with increasing r and $1/L$. The fidelities can be greatly optimized with respect to the standard teleportation scheme (STS with $g_q = g_p = 1$ and $\theta = \pi/4$; see short dash-dot-dot lines). Especially for a smaller L (e.g., $L = 0.1$), the optimal fidelity can almost access unity. While for a larger L (e.g., $L = 300$), the optimal fidelity approaches a value (less than one but still larger than 0.8), which is still superior to that in the STS. In Fig. 3(b), we consider the effect of different values of T on the optimal fidelity at $\kappa t = 0,0.2$. It is shown that

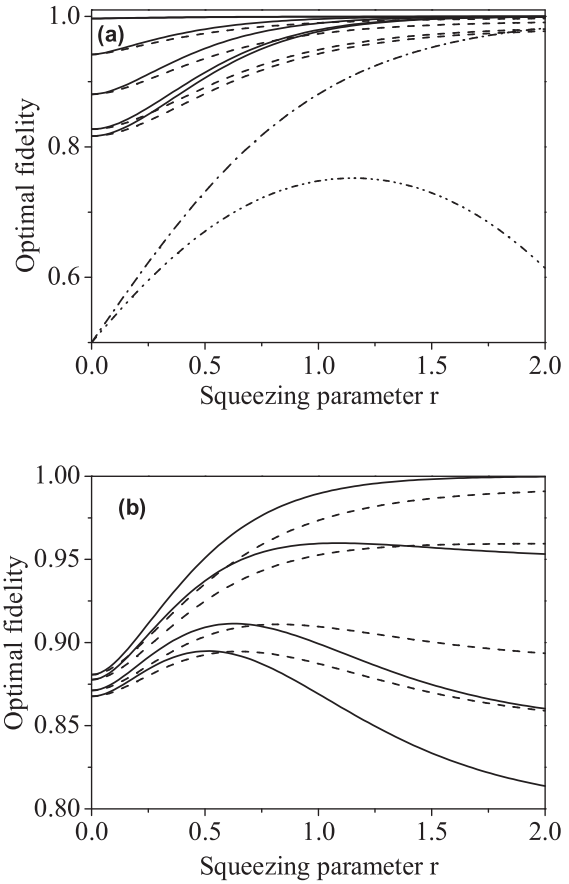

FIG. 3. The optimal fidelity for teleporting coherent states (CSs) as a function of r with $\bar{n} = 0$, $\kappa t = 0,0.2$ corresponding to solid and dash lines, respectively. (a) $L = 0.1,0.5,1,3,300$ and $T = 1$; for comparison, the teleportation in the STS is also plotted as dash-dot and dash-dot-dot lines for $\kappa t = 0,0.2$; (b) $T = 1,0.95,0.9,0.85,0.8$ and $L = 1$. The corresponding lines are arranged from top to bottom with the increasing L and $1/T$ for a given κt.

the optimal values decease with increasing $1/T$ for a given κt; while for the case of $T \neq 1$, by comparing the fidelities at $\kappa t = 0,0.2$ for a given T, it is found that the optimal fidelities first increase and then decrease with increasing r, and it is interesting to note that the optimal fidelity with $\kappa t = 0.2$ is superior to that with $\kappa t = 0$ when r exceeds a certain value. This indicates that our scheme may protect the teleportation fidelity from noise.

To see more clearly whether this scheme has the ability against the decoherence by using these tunable parameters, we plot here the optimized fidelity as a function of the evolution time κt for some different L with $\bar{n} = 0$, $r = 0.8$, and $T = 0.9$. Figure 4 shows that the fidelity by optimizing the three tunable parameters remains above 0.8 even for large value of κt. The result is true even for the limitation of $L \to \infty$. The teleported fidelities in the standard teleportation scheme (with $g_q = g_p = 1$ and $\theta = \pi/4$) are shown in the dashed lines in Fig. 4. We see that the optimized fidelities by three tunable parameters present higher ability against the decoherence than those in the standard teleportation scheme.

In addition, we compare the optimal effects of three tunable parameters. In Fig. 5, we plot the optimized fidelity over

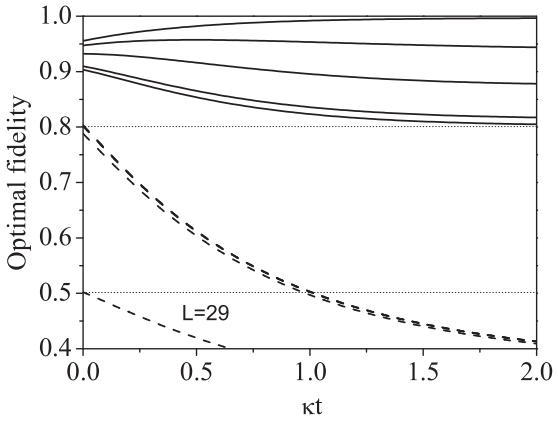

FIG. 4. The optimal fidelity for teleporting CSs as a function of κt with $\bar{n} = 0$, $r = 0.8$, $T = 0.9$ and $L = 0.1$, 0.5, 1, 3, 300 from top to bottom, respectively. The dashed lines are the results in the standard teleportation scheme.

different tunable parameters as a function of squeezing parameter r for a given $L = 1$ with $T = 1$, $\bar{n} = 0$, and $\kappa t = 0.2$. It is found that the optimization by three tunable parameters is the best when compared to single- and two-parameter optimization, especially when r is small. Thus, it is necessary to perform a simultaneous balanced optimization over these three parameters to obtain a maximization of teleportation fidelity for the probability distribution in Eq. (35).

B. Optimal fidelity for teleporting coherent states on a circle

In this section, we consider the optimal fidelity for teleporting CSs on a circle, i.e., $\epsilon = |\epsilon|e^{i\varphi} \equiv Ae^{i\varphi}$ with a fixed amplitude $|\epsilon| = A$ and unknown phase φ. In this case, the distribution function is $P(A,\varphi) = \delta(|\epsilon| - A)/2\pi$ which satisfies the normalization condition $\int_0^\infty \int_0^{2\pi} P(A,\varphi)d|\epsilon|d\varphi = 1$. In this case, the average teleportation fidelity can be calculated as

$$\bar{\mathcal{F}}_{\rm circle} = \frac{e^{-R_1}}{\sqrt{G}} \sum_{k=0}^{\infty} \frac{(R_2)^{2k}}{k!k!}, \tag{39}$$

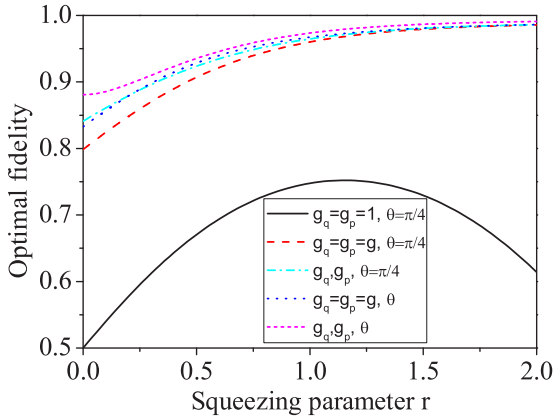

FIG. 5. The optimal fidelity for teleporting CSs as a function of r with $\bar{n} = 0$, $\kappa t = 0.2$, $T = L = 1$ for three tunable optimization parameters.

where $R_1 = A^2\{K_1[(1-f_1)^2 + f_2^2] + 4K_2(1-f_1)f_2\}/G$, $R_2 = A^2\{K_1(1-f_1)f_2 + K_2[(1-f_1)^2 + f_2^2]\}/G$, and $G = K_1^2 - 4K_2^2$. Maximizing $\bar{\mathcal{F}}_{\rm circle}$ over these three tunable parameters, we can get the optimized fidelity $\bar{\mathcal{F}}_{\rm circle}^{\rm opt} = \max_{g_q,g_p,\theta} \bar{\mathcal{F}}_{\rm circle}(r,g_q,g_p,\theta)$. Our numerical calculations show that, for the circle probability distribution, the maximum fidelity can be achieved when $g_q = g_p = g$ and $\theta = \pi/4$, which is different from the case in Sec. V A. Under this condition we have $f_1 = f_3 = g\sqrt{T}$ and $f_2 = f_4 = 0$, as well as $R_2 = K_2 = 0$. Thus the optimized fidelity is given by

$$\bar{\mathcal{F}}_{\rm circle}^{\rm opt} = \frac{1}{\Theta} \exp\left\{-\frac{A^2}{\Theta}(1 - g\sqrt{T})^2\right\}, \tag{40}$$

where we have set $\Theta = \Gamma + [g^2(R+1) + 1 + (g\sqrt{T} - e^{-\kappa t})^2 \cosh 2r + 2g\sqrt{T}e^{-\kappa t}e^{-2r}]/2$. It is obvious that $\Theta > 0$. In particular, Eq. (40) reduces to Eq. (33) in Ref. [28] when $\kappa t = 0$ and $T = 1$.

Using Eq. (39) or (40), we plot the optimal fidelity as a function of squeezing parameter r for some different values of A and T in Fig. 6. In Fig. 6(a), we consider the optimal fidelities with some different values of A with $T = 1$, $\bar{n} = 0$

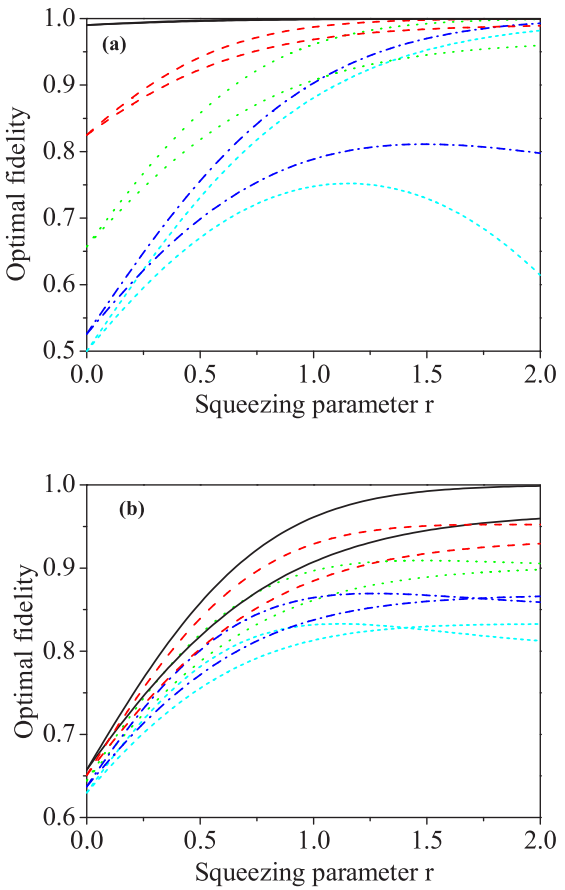

FIG. 6. The optimal fidelity for teleporting CSs as a function of r with $\bar{n} = 0$, $\kappa t = 0, 0.2$ (a) $A = 0.1$, 0.5, 1, 3, 300, and $T = 1$; (b) $T = 1$, 0.95, 0.9, 0.85, 0.8, and $A = 1$. For each optimized case (associated with a special plot style), the corresponding lines are arranged from top to bottom with the increasing A and $1/T$ at the point $r = 0$, respectively. For each plot style, the upper curve is for $\kappa t = 0$ while the lower curve is for $\kappa t = 0.2$.

as well as $\kappa t = 0, 0.2$. From Fig. 6(a), we can see that the optimal fidelities grow monotonically with increasing r for $\kappa t = 0$, but for $\kappa t = 0.2$ the optimal fidelities first increase and then decrease with increasing r, especially for a large A (say $A = 3$). In addition, for a small A, the optimal fidelity almost approaches unity. In Fig. 6(b), we also examine the effect of different T on the fidelity. It is interesting to notice that the optimal fidelity with $\kappa t = 0.2$ can be better than that with $\kappa t = 0$ when the squeezing r exceeds a certain value. This case is similar to that in Fig. 3(b). In Fig. 6, the point $r_{\max}$ corresponding to the maximum fidelity depends on κt and, for given κt, A, and T, the value of $r_{\max}$ can be determined by taking $\partial \bar{\mathcal{F}}^{\text{opt}}_{\text{circle}}/\partial r = 0$, which leads to

$$\{\Theta - A^2(1 - g\sqrt{T})^2\}\frac{\partial \Theta}{\partial r} = 0. \tag{41}$$

After a straightforward calculation, we obtain

$$\tanh 2r_{\max} = \frac{2g\sqrt{T}e^{-\kappa t}}{g^2 T + e^{-2\kappa t}}. \tag{42}$$

or

$$e^{4r_{\max}} - be^{2r_{\max}} + c^2 = 0, \tag{43}$$

where $b = 4[A^2(1 - g\sqrt{T})^2 - \Gamma]/(g\sqrt{T} - e^{-\kappa t})^2$, and $c = (g\sqrt{T} + e^{-\kappa t})/(g\sqrt{T} - e^{-\kappa t})$. In particular, when $g = 1/\sqrt{T}$ the fidelity is independent of the amplitude A and since $\Theta > 0$, the value of $r_{\max}$ in Eq. (42) reduces to that in Eq. (34).

In Fig. 7, choosing the same values of parameters T, r, and $\bar{n}$ as in Fig. 4, we plot the optimal fidelity as a function of κt. For comparison, we also plot the fidelity without the optimization, i.e., $g_q = g_p = 1$ and $\theta = \pi/4$ (see dashed lines). Figure 7 shows that the teleportation fidelity can be always above the classical limit 0.5 up to a large value of κt ($\leqslant 2$) when the amplitude A is less than about 1.7. When $A > 1.7$, it can go below the 0.5 for $A > 1.7$ when κt exceeds a certain threshold value. The optimal fidelities with $A = 15, 300$ are indistinguishable. In the STS, the fidelity is less than 0.5 when $A > 15$. Comparing the fidelities with and without optimization, it is shown that the former have better teleportation performance than the latter. However, this improvement is not as good as that shown in Fig. 4 where the optimal fidelities are over 0.8 for any L and $\kappa t \leqslant 2$.

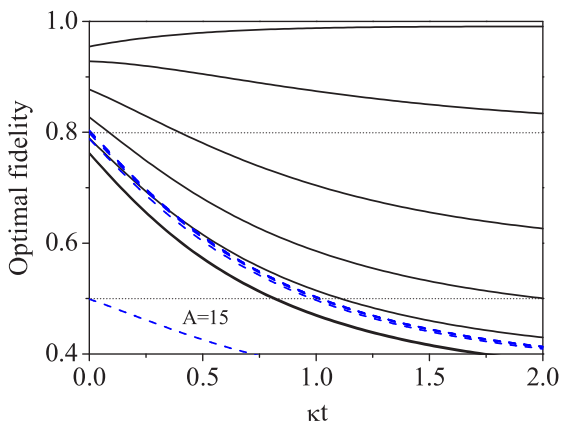

FIG. 7. The optimal fidelity for teleporting CSs as a function of κt with $\bar{n} = 0$, $r = 0.8$, $T = 0.9$ and $A = 0.1$, 0.5, 1, 1.7, 3, 300 from top to bottom, respectively. The dashed lines are the results in the standard teleportation scheme.

C. Optimal fidelity for teleporting coherent states by two-dimensional Gaussian distribution

In this section, we consider another probability distribution—the two-dimensional (2D) Gaussian distribution. The corresponding distribution is given by $P(\alpha) = 1/(\pi\chi)\exp[-|\alpha|^2/\chi]$ satisfying $\int P(\alpha)d^2\alpha = 1$ [18,20,32], where the variance parameter χ determines the cutoff of the amplitude α. By using Eqs. (21) and (24), the averaged fidelity can be calculated as

$$\bar{\mathcal{F}}_G = \frac{1}{\sqrt{H(g_p, \cos\theta) + \chi(1 - \sqrt{2T}g_p \sin\theta)^2}} \times \frac{1}{\sqrt{H(g_q, \sin\theta) + \chi(1 - \sqrt{2T}g_q \cos\theta)^2}}, \tag{44}$$

where the function $H(x,y)$ is defined in Eq. (28) [$(K_1 + 2K_2) = H(g_q, \sin\theta)$, $(K_1 - 2K_2) = H(g_p, \cos\theta)$]. Notice that the parameters g_q and g_p are independent from each other in Eq. (44), thus it is not difficult to obtain the optimal parameters by calculating $\partial\bar{\mathcal{F}}_G/\partial g_q = \partial\bar{\mathcal{F}}_G/\partial g_p = \partial\bar{\mathcal{F}}_G/\partial\theta = 0$. The optimal value is given by $\theta = \pi/4$ and $g_q = g_p = g$, where g is

$$g = \frac{\sqrt{T}(e^{-\kappa t}\sinh 2r + 2\chi)}{2[1 + T(\sinh^2 r + \chi)]}. \tag{45}$$

At this optimal point, the average optimized fidelity can be expressed as

$$\bar{\mathcal{F}}^{\text{opt}}_G = \frac{1}{H(g, 1/\sqrt{2}) + \chi(1 - g\sqrt{T})^2}. \tag{46}$$

It is clearly seen that the optimal factor g depends not only on T, but also on the evolution time κt. In particular, when $T \to 1$ and $\kappa t \to 0$, Eq. (45) reduces to the result in

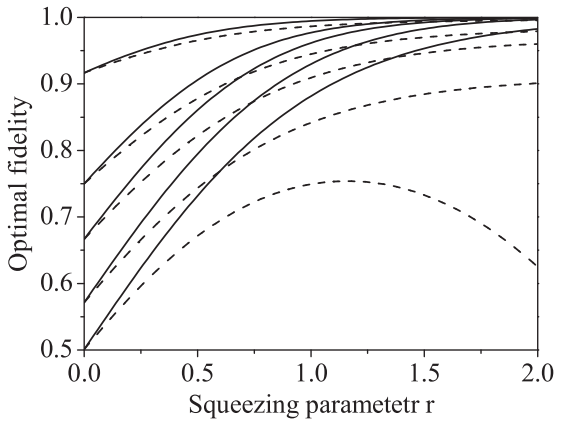

FIG. 8. The optimal fidelity for teleporting CSs as a function of r with $\bar{n} = 0$, $T = 1$, $\chi = 0.1$, 0.5, 1, 3, 300, and $T = 1$. For each optimized case (associated with a special plot style), the corresponding lines are arranged from top to bottom with the increasing χ. $\kappa t = 0, 0.2$ corresponds to solid and dash lines, respectively.

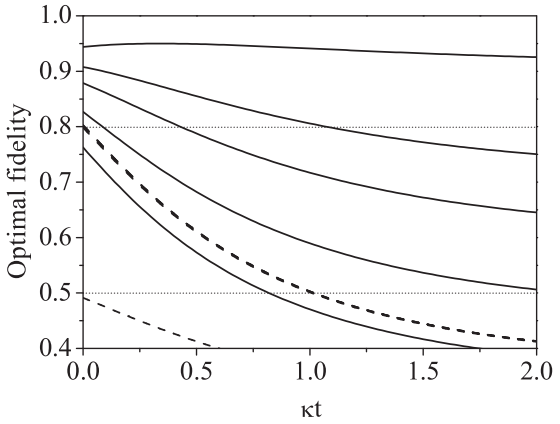

FIG. 9. The optimal fidelity for teleporting CSs as a function of κt with $\bar{n} = 0$, $r = 0.8$, $T = 0.9$, and $\chi = 0.1$, 0.5, 1, 3, 300 from top to bottom, respectively. For comparison, the fidelities with $g = 1$ are plotted here (dash lines).

Refs. [28,33]. In addition, in the limit $\chi \to \infty$ which implies that the probability distribution includes the whole complex plane, we have $g \to 1/\sqrt{T}$, which corresponds to the fidelity independent of ϵ.

Using Eq. (44) or (46), we plot the optimal fidelity as a function of squeezing parameter r and κt for some different values of χ in Figs. 8 and 9, respectively. From Fig. 8, we see that the smaller the distribution χ is, the higher the optimal fidelity is. As χ increases, which implies that we have less knowledge of the amplitude of the teleported states, the optimal fidelity approaches to that in the standard scheme ($g = 1$). In addition, as r increases, the fidelity first increases up to $r_{\max}$, and then decreases for a larger values of r for a given big $T\chi$. Actually, by using $\partial \bar{\mathcal{F}}_G^{\text{opt}}/\partial r = 0$, we get

$$e^{2r_{\max}} = \frac{(e^{\kappa t} + 1)T\chi + 1}{(e^{\kappa t} - 1)T\chi - 1}. \tag{47}$$

For instance, when $T = 1$, $\chi = 300$, and $\kappa t = 0.2$, then $r_{\max} \simeq 1.16$, which is in agreement with the numerical result in Fig. 8. In Fig. 9, we also consider the effect of decoherence on the fidelity. We can see that the results are similar to those for the case of circle distribution. Among the three distributions used above, the line distribution presents the most improvement for fidelity, while the Gaussian distribution presents the least improvement. Nevertheless, for three cases it is clearly shown that the fidelity of CV teleportation can be improved by using the tunable parameters even in a noise environment when compared with the standard teleportation scheme.

VI. CONCLUSIONS

In this paper, we examine the performance of three-tunable parameters in realistic scheme of CV quantum teleportation with input coherent states and the TMSV entangled resources. For our purpose, we derive the input and output relation in the CF formalism, which is convenient for calculating the teleportation fidelity for non-pure state inputs and any entangled resources. In this realistic scheme, including the noise effects and imperfect Bell measurements, we have derived the condition that the fidelity is independent of the amplitude of input coherent states for any entangled resource. To investigate the effect of three-tunable parameters on the fidelity of teleportation in the nonideal scheme, we derived the analytical expressions of the optimal fidelity for input coherent states with three different probability distributions. It is theoretically shown that the usefulness of tunable parameters for improving the fidelity of teleportation with or without the effect of environment and imperfect measurements. In particular, for the input coherent states with a linear distribution, the optimization with three tunable parameters is the best one with respect to single- and two-parameter optimization, especially in the region of small squeezing.

It would be interesting to extend the present analysis to teleport two-mode states (ideal or nonideal cases) by using multipartite (non-) Gaussian entangled resources in the formalism of CF. In addition, a recent comparison between the well-known CV VBK scheme and the recently proposed hybrid one by Anderson and Ralph (AR) has been made [34,35]. It is shown that the VBK teleportation is actually inferior to the AR teleportation within a certain range, even when considering a gain tuning and an optimized non-Gaussian resource. Thus it may be worthwhile considering whether these three-parameter optimizations can further improve the fidelity in the VBK scheme over that in the AR scheme, especially in the nonideal scheme.

ACKNOWLEDGMENTS

This work is supported by a grant from the Qatar National Research Fund (QNRF) under the NPRP Project 7-210-1-032. L.Y. Hu is supported by the China Scholarship Council (CSC) and the National Natural Science Foundation of China (Grants No.11264018 and No. 11464018), as well as the Natural Science Foundation of Jiangxi Province of China (Grant No. 20151BAB212006).

[1] C. H. Bennett, G. Brassard, C. Crépeau, R. Jozsa, A. Peres, and W. K. Wootters, Phys. Rev. Lett. **70**, 1895 (1993).
[2] L. Vaidman, Phys. Rev. A **49**, 1473 (1994).
[3] S. L. Braunstein and H. J. Kimble, Phys. Rev. Lett. **80**, 869 (1998).
[4] M. S. Zubairy, Phys. Rev. A **58**, 4368 (1998).
[5] A. Ourjoumtsev, A. Dantan, R. Tualle-Brouri, and P. Grangier, Phys. Rev. Lett. **98**, 030502 (2007).
[6] T. Opatrný, G. Kurizki, and D.-G. Welsch, Phys. Rev. A **61**, 032302 (2000).
[7] P. T. Cochrane, T. C. Ralph, and G. J. Milburn, Phys. Rev. A **65**, 062306 (2002).
[8] A. Kitagawa, M. Takeoka, M. Sasaki, and A. Chefles, Phys. Rev. A **73**, 042310 (2006).
[9] S. Y. Lee, S. W. Ji, and C. W. Lee, Phys. Rev. A **87**, 052321 (2013).

[10] T. J. Bartley, Philip J. D. Crowley, A. Datta, J. Nunn, L. J. Zhang, and I. Walmsley, Phys. Rev. A **87**, 022313 (2013).
[11] J. Fiurasek, Phys. Rev. A **84**, 012335 (2011).
[12] C. Navarrete-Benlloch, R. Garcia-Patron, J. H. Shapiro, and N. J. Cerf, Phys. Rev. A **86**, 012328 (2012).
[13] S. L. Zhang and P. van Loock, Phys. Rev. A **84**, 062309 (2011).
[14] L. Y. Hu, X. X. Xu, and H. Y. Fan, J. Opt. Soc. Am. B **27**, 286 (2010).
[15] S. Y. Lee and H. Nha, Phys. Rev. A **82**, 053812 (2010).
[16] S. Y. Lee, S. W. Ji, H. J. Kim, and H. Nha, Phys. Rev. A **84**, 012302 (2011).
[17] F. Dell'Anno, S. De Siena, L. Albano, and F. Illuminati, Phys. Rev. A **76**, 022301 (2007).
[18] F. Dell'Anno, S. De Siena, and F. Illuminati, Phys. Rev. A **81**, 012333 (2010).
[19] A. Vukics, J. Janszky, and T. Kobayashi, Phys. Rev. A **66**, 023809 (2002).
[20] P. T. Cochrane and T. C. Ralph, Phys. Rev. A **67**, 022313 (2003).
[21] A. Furusawa, J. L. Sørensen, S. L. Braunstein, C. A. Fuchs, H. J. Kimble, and E. S. Polzik, Science **282**, 706 (1998).
[22] A. V. Chizhov, L. Knöll, and D.-G. Welsch, Phys. Rev. A **65**, 022310 (2002).
[23] S. Takeda, T. Mizuta, M. Fuwa, H. Yonezawa, P. van Loock, and A. Furusawa, Phys. Rev. A **88**, 042327 (2013).
[24] A. V. Chizhov, JETP Lett. **80**, 711 (2004).
[25] S. Takeda, M. Fuwa, P. van Loock, and A. Furusawa, Phys. Rev. Lett. **114**, 100501 (2015).
[26] S. Takeda, T. Mizuta, F. Maria, P. van Loock and A. Furusawa, Nature (London) **500**, 315 (2013).
[27] S. Pirandola, J. Eisert, C. Weedbrook, A. Furusawa, and S. L. Braunstein, Nat. Photon. **9**, 641 (2015).
[28] F. S. Luiz and G. Rigolin, Ann. Phys. (NY) **354**, 409 (2015).
[29] P. Marian and T. A. Marian, Phys. Rev. A **74**, 042306 (2006).
[30] C. W. Gardiner and P. Zoller, *Quantum Noise* (Springer, Berlin, 2000).
[31] J. X. Zhang, C. D. Xie, F. L. Li, S. Y. Zhu, and M. S. Zubairy, Europhys. Lett. **56**, 478 (2001).
[32] S. L. Braunstein, C. A. Fuchs, and H. J. Kimble, J. Mod. Opt. **47**, 267 (2000).
[33] S. L. Braunstein, C. A. Fuchs, H. J. Kimble, and P. van Loock, Phys. Rev. A **64**, 022321 (2001).
[34] I. Kogias, S. Ragy, and G. Adesso, Phys. Rev. A **89**, 052324 (2014).
[35] U. L. Andersen and T. C. Ralph, Phys. Rev. Lett. **111**, 050504 (2013).